PROCEEDINGS, 48th Workshop on Geothermal Reservoir Engineering
Stanford University, Stanford, California, February 6-8, 2023
SGP-TR-224

# Conductive Proppants to Improve Heat Extraction

Sai Liu, Faras Al Balushi, Arash Dahi Taleghani

Department of Energy and Mineral Engineering, The Pennsylvania State University, University Park, PA 16802, United States

sailiu@psu.edu

fja5092@psu.edu

Arash.Dahi@psu.edu

**Keywords:** Closed-loop geothermal systems, heat extraction performance, hydraulic fracture, proppants

**ABSTRACT**

Geothermal energy has the potential to become a widespread reliable energy source. Traditionally, the conventional geothermal systems require a continuous supply of water, which limits their application in dry areas and causes risks such as induced seismicity. To circumvent this shortcoming, closed-loop geothermal systems not requiring water circulation have been proposed in recent years. However, heat extraction efficiency of closed-loop systems is limited due to the small heat exchange area between working fluid in the wellbore and surrounding rock. Therefore, it is of great importance to explore designs to improve heat extraction efficiency, thus increasing economic benefits. To enhance heat extraction efficiency, a fractured closed-loop geothermal system (FCLGS) is discussed in this paper. The objective of FCLGS is to improve heat transfer from hot rock to the wellbore by a conductive fracture. We utilize microscale numerical analysis to determine the best combination of proppants and coatings that yields the highest effective thermal conductivity of a proppant bed. To evaluate heat extraction performance of the FCLGS, a coupled three-dimensional model was established utilizing the finite element method and numerical simulations were conducted. Based on simulation results, the effects of different design factors on heat extraction were determined.

## 1. INTRODUCTION

Due to exploiting and consuming fossil fuels, such as oil and gas, many environmental problems have been induced in the past years including emissions and water pollution. To mitigate the problem, it is necessary to explore clean and renewable energy resources. Geothermal energy shows a promising prospect of developing into one of such resources. To extract thermal energy from the subsurface formations, the approach frequently adopted is to drill a well into rock formations with high enough temperature and inject a cold circulation fluid (typically water) and produce it as hot water or steam. Initially, producing hot water from the subsurface was realized by the open-loop system. However, sufficient circulation fluid is indispensable to extract thermal power using this kind of system. In order to promote fluid circulation in the subsurface, Enhanced Geothermal Systems (EGS) have been developed over the years. The principle behind EGS is to extract heat by generating a subsurface fracture system to which water can be supplemented continuously through injection wells. Cold water injected into the wellbore is heated sufficiently by surrounding high-temperature rock, after which hot water is generated at the production wells. To create an enhanced or engineered geothermal system, natural permeability of rock needs to be enhanced by hydroshearing or hydraulic fracturing techniques. Also, enough water supply is essential to ensure effective fluid circulation in the system (Kazemi et al., 2019; Pollack and Mukerji, 2019; Zhang and Zhao, 2020). Seismicity is another significant problem that prevents these systems from being applied in certain regions (Knoblauch and Trutnevyte, 2018; Andrés et al., 2019; Rathnaweera et al., 2020).

The open-loop systems possess some advantages resulting from the fluid circulation regime in the systems. First, reservoir rock is one component of the fluid circulation conduit, so a horizontal well is not required, and the costs of drilling can be cut down. Also, because of forced convection usually enhanced by fractures in EGS, the heat transfer rate from the reservoir to working fluid in the wellbore is significant. Despite the aforementioned advantages, there also exist limitations with open-loop systems. A well-noticed issue is that continuous supply of water is required during the whole heat extraction process (Dahi Taleghani, 2013). This prevents it from being employed in dry areas and results in environmental challenges like seismicity and waste water disposal.

To avoid these shortcomings, closed-loop geothermal systems, where continuous water supply is not required, have been developed in recent years. In closed-loop systems, working fluid is insulated and only circulated in the wellbore, thus avoiding direct contact with rock, so there is no working fluid loss into the reservoir. Closed-loop systems have the potential to be applied extensively. Santos et al. (2022) comprehensively summarized various geothermal systems that could be utilized for repurposing abandoned oil and gas wells. Because the temperature gradient is low in regions where the abandoned wells are located, adopting closed-loop systems is appropriate from the technical and economic perspective. Some research has been done to investigate heat extraction through closed-loop systems from different aspects. Bu et al. (2012) proposed a numerical model to quantitatively analyze the thermal power of a closed-loop system built from abandoned oil and gas wells. However, they explored the effect of only the fluid mass flow rate on heat extraction. By incorporating hydraulic fractures filled with proppants of high thermal conductivity, Ahmadi and Dahi Taleghani (2016) analyzed the possibility of improving heat extraction from closed-loop systems by fractures. To further understand the mechanism controlling the performance of a closed-loop system, Liu and Dahi Taleghani (2023) conducted a dimensionless analysis and derived dimensionless numbers that

comprehensively evaluate the effects of different factors impacting heat extraction. Wang et al. (2021a) proposed a closed-loop system with multiple laterals and studied the effect of the number of lateral wellbores on heat extraction performance, but it is challenging to build such a complicated system in terms of drilling technology. Wang et al. (2021b) and Bidarmaghz and Narsilio (2022) quantitatively investigated the impact of convection on heat extraction efficiency of closed-loop systems; nonetheless, the high rock permeability adopted in these studies is rare in deep rock.

Although previous studies have explored heat extraction efficiency of closed-loop systems with various focuses, there are still some gaps regarding this topic. Heat extraction of closed-loop systems is still limited to some extent. For instance, previous studies only considered basic closed-loop systems, namely without a fracture. The potential for improving heat extraction by altering the near-wellbore configuration has not been evaluated. To fill in the research gaps mentioned above, in this paper, a coupled three-dimensional model of a fractured closed-loop geothermal system (FCLGS) was built using the finite element method. With this model, a series of numerical simulations were conducted to investigate heat extraction efficiency under different design parameters. Before simulating heat extraction from the FCLGS, different proppant materials and conductive proppant coatings were tested through pore-scale modeling to determine the combination of proppant/coating that yields the highest effective thermal conductivity.

## 2. EFFECTIVE THERMAL CONDUCTIVITY OF PROPPANT BED

### 2.1 Numerical Model

In this paper, we use microscale analysis to investigate the impact of various proppant materials and conductive coatings to choose a combination yielding highest effective thermal conductivity. The combination with highest thermal conductivity is then used to perform field-scale analysis to determine its impacts on the heat extraction efficiency from a fractured closed-loop geothermal system (FCLGS). Analytical and numerical approaches to generate granular packs for numerical modeling typically simplify the geometry of grains or particles by perfect spheres. Such simplification yields a simple geometry that does not represent the complex textural and structural characteristics of actual granular particles including particles' size, sorting, and shape. In this research, we try to mimic the actual geometry of proppants by using discrete element method (DEM) and utilize Perlin noise amplitude to perturb spherical particles to yield realistic particles' shape.

Using DEM, we generated a proppant pack that resembles a 20/40 mesh with a particle size distribution shown in **Figure 1a**. The generated sample has dimensions of 9.15 mm × 2.82 mm × 4.67 mm (1016 × 313 × 518 voxels). The initial porosity of the proppant sample is 34.52% and the permeability is 301.6 Darcy. The proppant particles used in this study are non-spherical particles with Perlin noise amplitude of 0.20. Perlin noise amplitude controls the sphericity of the particles by stochastically perturbing the particle shape while holding the particle's volume constant (**Figure 1b**). The generated sample from DEM are exported in the form of stack of images similar to micro-Computed Tomography images obtained by scanning a physical sample.

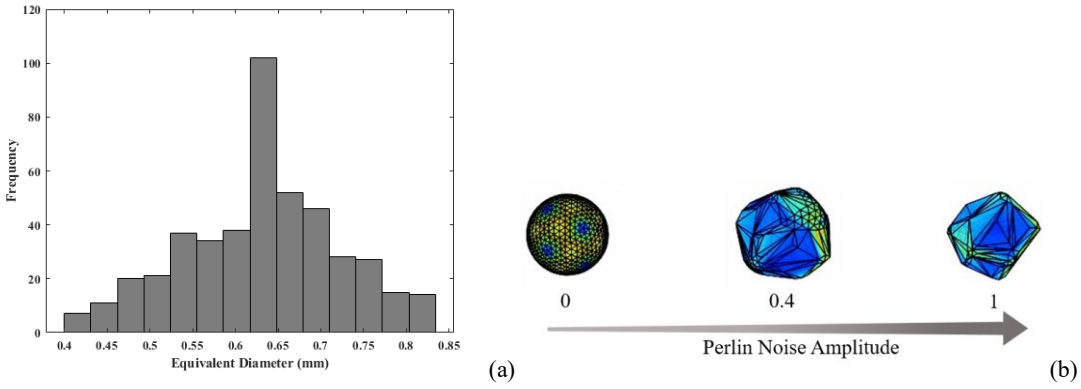


**Figure 1: (a) Particle size distribution of the samples generated and (b) particles shape based on Perlin noise amplitude are shown.**

We utilize image processing techniques to visualize and edit the stack of images representing the sample. To increase the thermal conductivity of the proppant pack, we apply a layer of conductive coating to the proppants. We construct two proppant packs with coating of different thickness. In the first sample, a 4-pixel erosion is applied to the particles and removed from the particles' boundaries. The removed part of the particles is then assigned as the coating and is added back to the proppant sample with different properties. The coating represents 39.63% by volume of the proppant particles. Another sample with thinner coating representing 9.57% by volume of the proppant particles was also generated where 1-pixel erosion is applied instead of 4-pixel erosion. We then use unstructured surface meshing where elements follow irregular pattern to construct our numerical mesh from the stack of binary images for finite element analysis. The generated mesh is enhanced by resolving any intersecting or incorrectly-oriented elements. In addition, the triangular and tetrahedron aspect ratios are kept below 20 to prevent the presence of low volume elements that can easily collapse during finite element simulations and lead to an early termination of the simulation. Since the upper bounds of the error in finite element analysis only depend on the smallest angle of the mesh elements (Persson and Strang, 2004; Lo, 2014), the most accurate results of finite element methods are obtained when the 2D triangles are equilateral (Field, 2000). Thus, the enhanced model is remeshed using the best isotropic triangles algorithm to reduce the number of elements and optimize the quality of the mesh by finding the best location for the nodes to yield isotropic triangles. **Figure 2** shows a schematic of the heat transfer analysis including the applied boundary conditions.

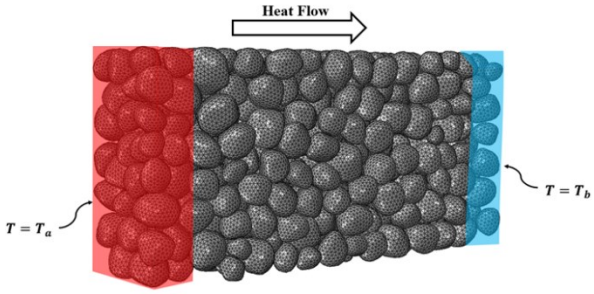


**Figure 2: Boundary conditions used for heat transfer analysis using finite element methods.**

### 2.2 Measurement Results

We tested different proppants and coating materials to determine the best combination of proppant and coating that yields the highest effective thermal conductivity. In addition, we investigated the impact of different friction coefficients and the stiffness of the proppant and coating on the resulting thermal conductivity. Here, a uniaxial compaction is applied where one boundary is fixed and a displacement load is applied on the opposite face of the sample. A maximum strain value of 5% is applied. The mechanical properties of the model used for the loading computations are shown in **Table 1**.

**Table 1: Mechanical properties of the sample with thick coating used in this simulation.**

| Property | Proppant | Coating |
|---|---|---|
| Material | Sand/quartz | Copper |
| $\rho\ (g/cm^3)$ | 2.65 | 8.96 |
| $E\ (GPa)$ | 70 | 130 |
| $\nu\ (-)$ | 0.25 | 0.34 |

Defining the behavior of the contact between proppant particles in finite element analysis is essential in determining overall heat transfer in the pack. Furthermore, without proper contact definition, particles may penetrate into each other if large deformations occur in the model and the resulting loading curve may be linear. Here, we define mechanical and thermal contacts. Mechanical contact includes Hertzian contact in the normal direction and frictional contact with a constant friction coefficient in the tangential direction. Thermal contact definition is also needed to define the mean of heat transfer. In this model, conductivity is defined in such a way that the particles that are not in contact do not transfer heat. Thus, thermal contact with infinite conductance is used between contacting particles so that heat is transmitted without additional resistance other than the intrinsic thermal resistance of coating material. To speed up FEM simulations and their accuracy, the mesh should be free of distorted elements, *i.e.* they should be tetrahedrons with low initial volumes or high aspect ratios. Mass scaling can also be used but should not result in a kinetic energy higher than 5% of the overall internal energy to ensure tolerable quasi-static analysis (Field, 2000).

Then, we compare the effective thermal conductivity of different combinations of proppant and coating properties. **Table 2** shows the effective thermal conductivity for each material. Here, we initially compact the sample to ensure proper packing of the sample. Next, we apply the desired closure stress while keeping the confinement of the sample. In the presented cases below, up to 5% of strain is applied axially until closure stress of 100 MPa is achieved. Without any coating, the effective thermal conductivity of the pack of sand proppants is computed to be 0.65 $W/mK$. Upon applying a thin coating of copper, the thermal conductivity increases to 32.75 $W/mK$, an increase of 50 times larger than the case of no coating. Thicker proppant coating is observed to increase the effective thermal conductivity to 50.05 $W/mK$, which is more than 77 times higher than the case of no coating. Aluminum Nitride proppant is found to yield the highest effective thermal conductivity of 60.89 $W/mK$ when coated with thick copper coating. Thus, Aluminum Nitride proppant with thick copper coating is considered for the field-scale analysis of the FCLGS.

**Table 2: Computed effective thermal conductivity for both proppant samples.**

| **Proppant** | **Coating** | **Effective Thermal conductivity ($\frac{W}{m\,K}$)** | |
|---|---|---|---|
| | | **Thin Coating** | **Thick Coating** |
| Sand (quartz) | No coating | 0.65 | 0.65 |
| Sand (quartz) | Copper | 32.75 | 50.05 |

| | | | |
|---|---|---|---|
| Bauxite | Copper | 30.73 | 47.45 |
| Aluminum Nitride | Copper | 45.31 | 60.89 |
| Sand (quartz) | Aluminum | 21.90 | 34.72 |
| Bauxite | Aluminum | 19.71 | 30.91 |
| Aluminum Nitride | Aluminum | 37.09 | 46.48 |

## 3. MODELLING OF THE SYSTEM

### 3.1 Geometric model

The geometric configuration of the model for a fractured closed-loop geothermal system (FCLGS) is illustrated in **Figure 3.** To better present the internal configuration of the system, surrounding rock was not plotted. To facilitate heat transfer from rock to the wellbore, a vertical double-wing fracture with high thermal conductivity is connected to the lower section of the wellbore, as shown in **Figure 3b**. Generally, the permeability of geothermal reservoir rock, such as granite, is very low and thus the magnitude of heat convection in the reservoir is much smaller than that of conduction. Hence, the effect of reservoir permeability on the efficiency of a closed-loop system is very limited and can be neglected (Beckers et al., 2022). Based on this three-dimensional FCLGS model, numerical simulations were performed using finite element method. The intended results are the production temperature, i.e., the temperature of fluid flowing out through the outlet of the output channel; and net power, which is the produced heat from the well per unit time after subtracting pumping power. The heat extraction performance of the FCLGS would be examined under different conditions to determine effects of some design parameters.

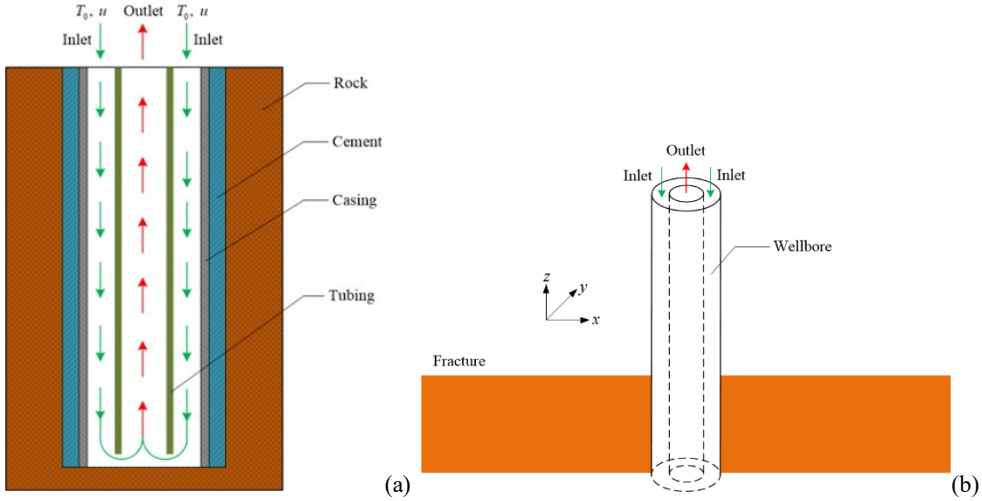


**Figure 3: Illustration of (a) basic wellbore profile and (b) 3D model of fractured closed-loop geothermal system.**

### 3.2 Governing equations for FCLGS

The main physics governing the problem is the heat transfer between different parts of the system in the subsurface. During the heat transfer process, thermal energy is transmitted through the reservoir, fracture, cement, casing, working fluid circulating inside the well, and the tubing used for insulation. The governing equations involved in this study are listed in the following parts. The energy conservation equation that describes heat transfer in the solids, including cement, casing, and tubing, is formulated as

$$\rho_s C_{p,s} \frac{\partial T_s}{\partial t} - \lambda_s \nabla^2 T_s = 0 \,, \tag{1}$$

where $T_s$ is the temperature of the solids; $t$ is the time; $\rho_s$ is the density of solids; $C_{p,s}$ is the heat capacity of solids under constant pressure; $\lambda_s$ is the thermal conductivity of solids. For circulating fluid in the wellbore, the energy conservation equation is formulated as

$$\rho_f C_{p,f} \frac{\partial T_f}{\partial t} + \rho_f C_{p,f} \mathbf{u} \nabla T_f - \lambda_f \nabla^2 T_f = 0 \,, \tag{2}$$

where $T_f$ is the temperature of the circulating fluid; $\rho_f$ is the density of the circulating fluid in the well; $C_{p,f}$ is the heat capacity of the circulating fluid; $\lambda_f$ is the thermal conductivity of the circulating fluid; $\mathbf{u}$ is the flow velocity of the circulating fluid. For heat transfer in the reservoir, porosity of the reservoir is taken into consideration, and it is assumed that the reservoir is saturated with underground water. The energy conservation equation for the reservoir, including the matrix and fracture, is formulated as

$$(\rho C_p)_{eff}\frac{\partial T_r}{\partial t} - \lambda_{eff}\nabla^2 T_r = 0\,, \tag{3}$$

where $T_r$ is temperature in the reservoir; $(\rho C_p)_{eff}$ is the effective heat capacity; $\lambda_{eff}$ is the effective thermal conductivity. The total thermal power obtained at the outlet is

$$P_{total} = \dot{V}\rho_f C_{p,f}(T_{out} - T_{in})\,,\ P_{net} = P_{total} - P_{pumping}\,, \tag{4}$$

where $\dot{V}$ is the fluid circulation rate in the wellbore; $T_{in}$ is the injection temperature of fluid at the inlet; $T_{out}$ is the output temperature of fluid at the outlet; $P_{pumping}$ is The pumping power consumed to overcome friction between working fluid. The governing equations listed above are discretized using the shape functions of the finite element method. Then, these equations are further discretized over the time domain. Finally, the discretized equations are solved by iteration using the Newton-Raphson method.

## 4. EVALUATION OF HEAT EXTRACTION PERFORMANCE

From the configuration of the fractured closed-loop geothermal system (FCLGS) in **Figure 3**, there are some critical factors impacting its heat extraction. To investigate heat extraction performance of the system, an example model was established, and numerical simulations were conducted. The basic parameters for the geometry and boundary conditions of the simulation model are listed in **Table 3**, and material parameters are given in **Table 4**. From **Table 2**, it has been known that the proppant bed of Aluminum Nitride with thick copper coating possesses the highest thermal conductivity of 60.89 $\mathrm{W/(m\cdot K)}$, so this thermal conductivity would be adopted for the fracture filled with proppants.

**Table 3: Parameters of geometry and boundary conditions used for the modeling.**

| Parameter (Unit) | Value | Parameter (Unit) | Value |
|---|---|---|---|
| Tubing outer diameter (mm) | 168.28 | Tubing inner diameter (mm) | 114.30 |
| Casing outer diameter (mm) | 244.48 | Casing inner diameter (mm) | 215.9 |
| Cement thickness (mm) | 20 | Well depth (m) | 5200 |
| Injection velocity (m/s) | 1.0 | Injection temperature $T_0$ (° C) | 50 |
| Reservoir temperature at well bottom (°C) | 300 | Reservoir temperature at top surface (°C) | 20 |
| Fracture half length (m) | 100 | Fracture height (m) | 400 |
| Fracture thickness (mm) | 60 | | |

**Table 4: Material parameters used in simulations.**

| Parameter (Unit) | Fracture | Rock | Tubing | Casing | Cement | Fluid |
|---|---|---|---|---|---|---|
| Density ($\mathrm{kg/m^3}$) | 2800 | 2800 | 900 | 7850 | 2400 | 998.2 |
| Thermal conductivity $\mathrm{[W/(m\cdot K)]}$ | 60.89 | 3.4 | 0.006 | 45 | 10 | 0.598 |
| Heat capacity $\mathrm{[J/(kg\cdot K)]}$ | 920 | 920 | 1800 | 490 | 920 | 6184 |
| Viscosity ($\mathrm{Pa\cdot s}$) | | | | | | 0.001 |

### 4.1 Effect of fluid circulation rate

During the operation of closed-loop systems, the circulation rate of working fluid in the wellbore can be adjusted. To explore the impact of the fluid circulation rate on heat extraction of the FCLGS, cases with different flow velocities of injected fluid were simulated. To change the fluid circulation rate, the flow velocity of injected fluid was varied from 1.0 m/s to 3.0 m/s in an arithmetic progression. **Figure 4** shows the time-dependent production temperature and net power by different flow velocities. As the velocity increases from 1.0 m/s to 2.0 m/s, production temperatures at different time decrease significantly, while net power is increased to a certain extent. As the velocity increases from 1.0 m/s to 2.0 m/s, the net power after 90 days is enhanced from 5.32 MW to 5.58 MW (by 4.89%). The net power after 180 days is increased from 4.63 MW to 4.79 MW (by 3.46%). However, as the velocity increases from 2.0 m/s to 3.0 m/s, net power starts to decrease. This is because pumping power becomes higher due to the increase in flow velocity. Although the total thermal power obtained is increased at the same time, the increase in pumping power is greater than that in total thermal power. Therefore, a higher fluid circulation rate is not always beneficial in terms of net power extracted. By the injection velocity of 2 m/s, the highest after-180-day net

power is obtained among this group of cases. In summary, if a high production temperature is preferred rather than high net power, then adopting a lower fluid circulation rate is recommended. In contrast, a higher fluid circulation rate is required if high net power is favored instead, but there exists a critical fluid injection velocity, beyond which the net power after 180 days starts to decline. Hence, it is necessary to ensure that the fluid circulation rate does not exceed the critical value.

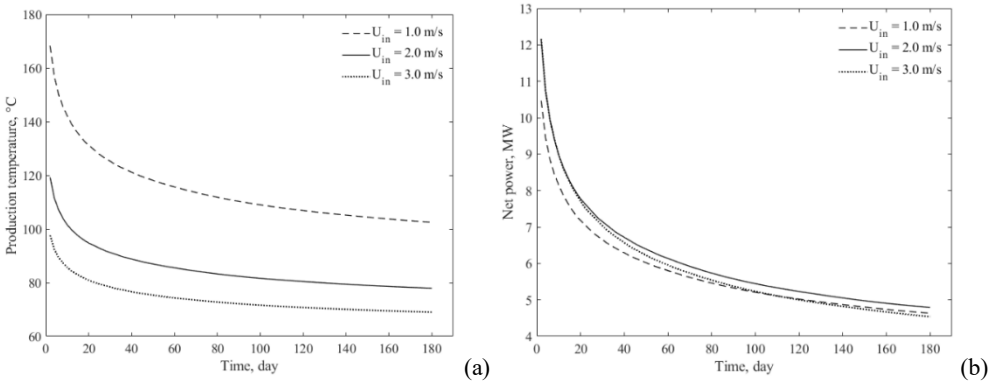


**Figure 4: Effect of flow velocity of injected fluid on (a) production temperature versus time; (b) net power versus time.**

### 4.2 Effect of working fluid heat capacity

Physical parameters of circulating fluid, such as heat capacity, might also have an impact on heat extraction performance. To understand how working fluid heat capacity affects heat extraction performance, several cases with different circulating fluid heat capacities were simulated. For these cases, the flow velocity of injected fluid is 1.0 m/s, while the heat capacity of working fluid is varied from $4184\ \mathrm{J/(kg\cdot K)}$ to $6184\ \mathrm{J/(kg\cdot K)}$. The time-related production temperature and net power obtained with different heat capacity values are displayed in **Figure 5**. It can be observed that with fluid heat capacity increasing, fluid production temperature decreases noticeably, while net power keeps increasing at a relatively slower rate. The reason for this result is that total thermal power obtained is directly proportional to fluid heat capacity. Although production temperature has been reduced due to heat capacity increasing, net power is still enhanced given increased total thermal power and unchanged pumping power. As fluid heat capacity increases from $4184\ \mathrm{J/(kg\cdot K)}$ to $6184\ \mathrm{J/(kg\cdot K)}$, the net power after 90 days is enhanced from 4.98 MW to 5.33 MW (by 7.03%). The net power after 180 days is increased from 4.37 MW to 4.63 MW (by 5.95%). Despite being not negligible, the magnitude of increase in net power is not significant. It can be concluded that there is a similarity between the effect of fluid heat capacity and that of the fluid circulation rate, although they are not the same. Compared to the effect of the fluid circulation rate, the production temperature varies relatively more linearly with respect to fluid heat capacity. However, increasing fluid heat capacity does not lead to higher pumping power, so there is not a critical fluid heat capacity beyond which net power decreases, which differs from the effect of the fluid circulation rate. Circulating fluid with high heat capacity is required if high net power is expected from the FCLGS. Conversely, if a high production temperature is the objective, then fluid with low heat capacity should be applied.

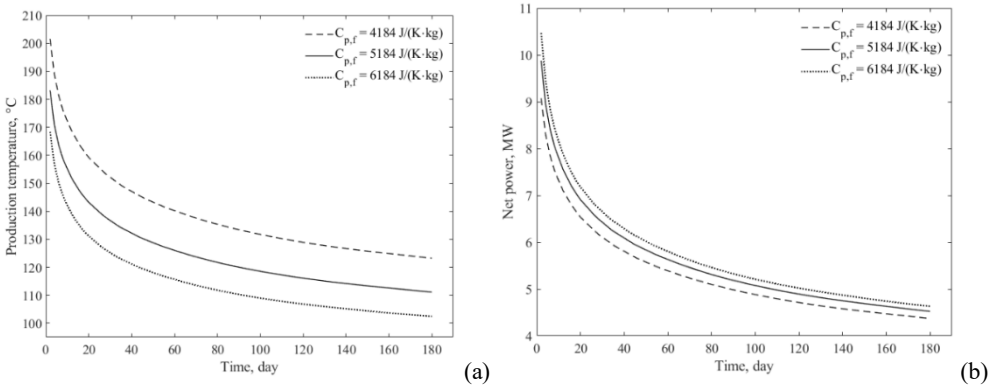


**Figure 5: Effect of working fluid heat capacity on (a) production temperature versus time; (b) net power versus time.**

## 5. CONCLUSIONS

In this paper, a fractured closed-loop geothermal system (FCLGS) was proposed to improve heat extraction performance of closed-loop systems. A numerical study was conducted to understand the effects of several design parameters on the heat extraction performance of the FCLGS. To simulate heat extraction performance of the FCLGS, a three-dimensional model that couples fluid flow and heat transfer in the wellbore was established using the finite element methods. To measure the effective thermal conductivity of a proppant bed, a microscale model was established first. Also, the effect of different proppant and coating materials was tested to determine the best combination of proppant and coating that yields the highest effective thermal conductivity. It is shown that Aluminum Nitride proppant

matrix with copper coating yields the highest thermal conductivity with a value of $45.31 W/(m \cdot K)$ for thin coating and $60.89 W/(m \cdot K)$ for thick coating. Then, by adopting the measured proppant bed thermal conductivity for the fracture, numerical simulations were performed to evaluate heat extraction performance of the FCLGS. It was found that a higher fluid circulation rate is required if high net power rather than high production temperature is expected, but there is a critical fluid injection velocity beyond which the net power after 180 days starts to decline. The effect of fluid heat capacity has a similarity to that of the fluid circulation rate. However, the production temperature varies relatively more linearly with respect to fluid heat capacity, and there is not a critical fluid heat capacity. The results and conclusions achieved in this paper can provide a reference for designing closed-loop systems in the future.

**REFERENCES**

Ahmadi, M., and Dahi Taleghani, A: Feasibility Study of Heat Extraction from a Closed-Loop Fractured Geothermal Reservoir; A Multiphysics Problem, Paper presented at the 50th U.S. Rock Mechanics/Geomechanics Symposium, Houston, TX (2016).

Andrés, S., Santillán, D., Mosquera, J.C., and Cueto-Felgueroso, L.: Thermo-Poroelastic Analysis of Induced Seismicity at the Basel Enhanced Geothermal System, Sustainability, 11, (2019), 6904.

Beckers, K.F., Rangel-Jurado, N., Chandrasekar, H., Hawkins, A.J., Fulton, P.M., and Tester, J.W.: Techno-Economic Performance of Closed-Loop Geothermal Systems for Heat Production and Electricity Generation, Geothermics, 100, (2022), 102318.

Bidarmaghz, A., and Narsilio, G.A.: Is natural convection within an aquifer a critical phenomenon in deep borehole heat exchangers' efficiency? Applied Thermal Engineering, 212, (2022), 118450.

Bu, X., Ma, W., and Li, H.: Geothermal Energy Production Utilizing Abandoned Oil and Gas Wells, Renewable Energy, 41, (2012), 80-85.

Dahi Taleghani, A.: An Improved Closed-Loop Heat Extraction Method from Geothermal Resources, Journal of Energy Resources Technology, 135, (2013), 042904.

Field, D.A.: Qualitative measures for initial meshes, International Journal for Numerical Methods in Engineering, 47(4), (2000), 887-906.

Kazemi, A.R., Mahbaz, S.B., Dehghani-Sanij, A.R., Dusseault, M.B., and Fraser, R.: Performance Evaluation of an Enhanced Geothermal System in the Western Canada Sedimentary Basin, Renewable and Sustainable Energy Reviews, 113, (2019), 109278.

Knoblauch, T.A.K., and Trutnevyte, E.: Siting enhanced geothermal systems (EGS): Heat benefits versus induced seismicity risks from an investor and societal perspective, Energy, 164, (2018), 1311-1325.

Liu, S., and Dahi Taleghani, A.: Factors affecting the efficiency of closed-loop geothermal wells, Applied Thermal Engineering, 222, (2023),119947.

Lo, D.S.: Finite element mesh generation, CRC Press, (2014).

Persson, P.O., and Strang, G.: A simple mesh generator in MATLAB, SIAM review, 46(2), (2004), 329-345.

Pollack, A., and Mukerji, T.: Accounting for subsurface uncertainty in enhanced geothermal systems to make more robust techno-economic decisions, Applied Energy, 254, (2019), 113666.

Rathnaweera, T.D., Wu, W., Ji, Y., and Gamage, R.P.: Understanding injection-induced seismicity in enhanced geothermal systems: From the coupled thermo-hydro-mechanical-chemical process to anthropogenic earthquake prediction, Earth-Science Reviews, 205, (2020), 103182.

Santos, L., Dahi Taleghani, A., and Elsworth, D.: Repurposing abandoned wells for geothermal energy: Current status and future prospects, Renewable Energy, 194, (2022), 1288-1302.

Wang, G., Song, X., Shi, Y., Yang, R., Yulong, F., Zheng, R., and Li, J.: Heat extraction analysis of a novel multilateral-well coaxial closed-loop geothermal system, Renewable Energy, 163, (2021a), 974-986.

Wang, G., Song, X., Song, G., Shi, Y., Yu, C., Xu, F., Ji, J., and Song, Z.: Analyzes of thermal characteristics of a hydrothermal coaxial closed-loop geothermal system in a horizontal well, International Journal of Heat and Mass Transfer, 180, (2021b), 121755.

Zhang, Y., and Zhao, G.F.: A global review of deep geothermal energy exploration: from a view of rock mechanics and engineering, Geomechanics and Geophysics for Geo-Energy and Geo-Resources, 6, (2020), 4.